

Robust Nonlinear Array Interpolation for Direction of Arrival Estimation of Highly Correlated Signals

Marco A. M. Marinho^{a,b,*}, Felix Antreich^c, Stefano Caizzone^d,
João Paulo C. L. da Costa^a, Alexey Vinel^b, Edison Pignaton de Freitas^e

^aUniversity of Brasília (UnB), Department of Electrical Engineering (ENE), Brasília, Brazil

^bHalmstad University, School of Information Technology, Halmstad, Sweden

^cDepartment of Teleinformatics Engineering - Federal University of Ceará (UFC), Fortaleza, Brazil

^dGerman Aerospace Center (DLR), Institute for Communications and Navigation, Wessling, Germany

^eFederal University of Rio Grande do Sul (UFRGS), Informatics Institute, Porto Alegre, Brazil

Abstract

Important signal processing techniques need that the response of the different elements of a sensor array has specific characteristics. For physical systems this often is not achievable as the array elements' responses are affected by mutual coupling or other effects. In such cases, it is necessary to apply array interpolation to allow the application of ESPRIT, Forward Backward Averaging (FBA), and Spatial Smoothing (SPS). Array interpolation provides a model or transformation between the true and a desired array response. If the true response of the array becomes more distorted with respect to the desired one or the considered region of the field of view of the array increases, nonlinear approaches become necessary. This work presents two novel methods for sector discretization. An Unscented Transform (UT) based method and a principal component analysis (PCA) based method are discussed. Additionally, two novel nonlinear interpolation methods are developed based on the nonlinear regression schemes Multivariate Adaptive Regression Splines (MARS) and Generalized Regression Neural Networks (GRNNs). These schemes are extended and applied to the array interpolation problem. The performance of the proposed methods is examined using simulated and measured array responses of a physical system used for research on mutual coupling in antenna arrays.

Keywords: Array Interpolation, Array Mapping, Antenna Arrays, Direction of Arrival Estimation

1. Introduction

Sensor arrays have been applied in various fields of modern electrical engineering. From up and coming applications such as massive Multiple Input Multiple Output (MIMO) [1] to microphone arrays capable, for instance, of detecting and separating multiple sound sources or playing individual songs depending on the seat of a car [2]. The mathematical tools provided by array signal processing together with the evolution of electronic circuitry have made such applications a reality. The problem of parameter estimation is of major interest in the field of array signal processing. Among the parameters that can be estimated, the direction of arrival (DOA) of an electromagnetic wave received at the array has experienced significant attention. Knowledge of the DOA is important for e.g. spatial filtering or source tracking.

Among the available methods for multiple DOA estimation, some of them stand out due to their computational

efficiency, such as the Iterative Quadratic Maximum Likelihood (IQML) [3], Root Weighted Subspace Fitting (Root-WSF) [4], Root-MUSIC [5], and ESPRIT [6]. These methods, however, demand very specific and precise responses from the antenna array, i.e. Vandermonde or left centro-hermitian responses. Another important use of arrays with such responses is that they provide the mathematical model necessary for the application of important tools such as Spatial Smoothing (SPS) [7] and Forward Backward Averaging (FBA) [8]. Model order selection methods [9, 10, 11, 12], used to estimate the number of received signals, have their performance highly impacted by the presence of correlated signals, making SPS and FBA necessary under such conditions. Methods such as Maximum Likelihood (ML) [13, 14] or its iterative implementations such as the Expectation Maximization (EM) [15, 16, 17] and the Space Alternating Generalized Expectation Maximization (SAGE) [18, 19, 20] do not require a specific array geometry, however, need precise knowledge of the model order. Furthermore, these methods are more computationally expensive and, in the case of EM and SAGE, can have convergence problems in the presence of local maxima.

Arrays that have a Vandermonde or a left centro-hermitian response are very hard to achieve in real sensor ar-

*Principal corresponding author

Email address: marco.marinho@ieee.org (Marco A. M. Marinho)

URL: <http://www.marcomarinho.com> (Marco A. M. Marinho)

ray implementations. Mutual coupling of the antennas, changes in antenna location, material tolerances, hardware biases, and the surrounding environment of the array all affect the response of individual antennas and, thus, of the antenna array. To deal with such imperfections, a mapping between the true and desired virtual array response can be created, and the received data can then be interpolated into this virtual array.

Creating a precise model for the entire field of view of the array is difficult, especially when applying linear interpolation to arrays with a limited number of antennas [21]. Therefore, array interpolation schemes rely on dividing the field of view of the array into smaller angular regions, called sectors [22]. In previous array interpolation works the so-called sector-by-sector processing is performed. The array is divided into multiple regions to be interpolated and these regions are discretized using a dense uniform grid. For each of these regions, a separate DOA estimation is performed. That is, interpolation is performed over a limited region of the field view of the array to keep the bias introduced by the interpolation limited. Larger transformation regions, in general, will result in less accurate interpolations. However, sector-by-sector processing introduces a number of problems e.g. separation of DOA estimates from different sectors, etc.

Array interpolation can be achieved in either a linear or nonlinear fashion. In case the true response strongly differs from the desired virtual response or the number of antennas is small, a nonlinear interpolation method becomes necessary. Under such demanding conditions, nonlinear array interpolation is capable of achieving a lower DOA estimation bias than compared to its linear counterpart.

In this work, a method for signal adaptive sector selection is presented and two different alternatives for sector discretization are developed. First, a novel method for sector discretization is derived from the Unscented Transform (UT) [23]. This mathematical transformation, mostly used in the context of Kalman filters, is extended to the problem of array interpolation to discretize the detected sectors. The statistical equivalence of the region transformed by the UT when compared to the true array input is proven. A second method extends the concept of principal component analysis (PCA), a tool commonly used in the context of regression in statistics, to the problem of discretizing the detected sectors in order to minimize problems with correlation in predictors and reduce the computational load necessary to build the interpolation methods.

Furthermore, also two novel methods for nonlinear interpolation based on nonlinear regression are developed. First, a method is derived from Multivariate Adaptive Regression Splines (MARS) [24], a nonlinear and nonparametric regression method. We are extending MARS to the problem of array interpolation by introducing an augmented formulation of the mapping and by deriving a pertinent generalized cross-validation to reduce the usually over-fitted models. This approach is suitable for arrays with responses that strongly differ from the desired re-

sponse and that have a small number of antennas. A second nonlinear interpolation approach extending the concepts of General Regression Neural Networks (GRNNs) [25] into the context of array interpolation is developed by using an augmented formulation of the mapping. The GRNN based method is able to model nonlinear relationships between the true and desired array responses at a lower computational cost compared to the MARS approach.

The efficiency and performance of the proposed approaches are tested by means of numerical simulations using measured responses of a real physical system, a linear array with a variable inter-element spacing for research on mutual coupling in antenna arrays. The performance of the proposed methods is also studied in case a simulated (ANSYS HFSS) response is used to build the interpolation models instead of the true measured data.

The remainder of this work is divided into seven sections. In Section 2 an overview of previous works on the topic of array interpolation and how they are related to the methods proposed in this work is presented. Section 3 details the data model used in this work. The concept of array interpolation as considered in this work and important related concepts are shown in Section 4. Section 5 addresses the methods for sector selection and discretization proposed in this work. The proposed nonlinear interpolation methods are presented in Section 6. Results from numerical simulations are shown in Section 7. Finally, in Section 8 conclusions are drawn.

2. Related Works

Bronez [26] first presented a solution for mapping true imperfect array responses into precise and desired responses, and he has called such mapping array interpolation. The presented schemes rely on dividing the field of view of the array response into smaller angular regions, called sectors. For each of these sectors, a transformation matrix is calculated using the empirical knowledge of the true array response. This is called sector-by-sector array interpolation, the larger the region transformed the larger will be the bias introduced due to transformation imprecision. Friedlander and Weiss [27] extended sector-by-sector array interpolation to include FBA, SPS, and DOA estimation algorithms such as Root-MUSIC [22]. Bühren et al. [21] presented a design metric for the virtual array seeking to preserve the directional characteristics of the true array. Bühren et al. [28] and Weiss and Gavish [29] presented methods for array interpolation that allow the application of ESPRIT for DOA estimation. All of these interpolation methods are performed on by sector-by-sector basis, dividing the entire field of view of the array and performing multiple DOA estimations, one for each sector.

When performing array interpolation for a sector there is no guarantee with respect to what happens with signals received from outside the angular region for which the transformation matrix was calculated (out-of-sector signals). If the out-of-sector signal is correlated with any pos-

sible in-sector signal, a large bias in the DOA estimation is introduced. Pesavento et al. [30] proposed a method for filtering out of sector signals using cone programming. A similar approach was used by Lau et al. [31, 32] where correlated out-of-sector signals were addressed by filtering out the out-of-sector signals.

More recently, array interpolation has been applied to more specific scenarios. Liu et al. [33] extended the concept of linear array interpolation to coprime arrays allowing for better identifiability of received signals. Hosseini and Sebt [34] applied the concept of linear array interpolation to sparse arrays by selecting virtual arrays as small as possible while retaining the aperture of the original sparse array.

This work proposes an adaptive single sector selection method aiming to circumvent the problem of out-of-sector signals by interpolating all regions of the array where power is received using a single transformation. The authors [35] studied an alternative for applying ESPRIT with FBA and SPS, relying on a signal adaptive sector construction and discretization and extended the method to the multidimensional case [36]. The proposed method prevents out-of-sector problems by building a single sector using a signal adaptive approach while also bounding the transformation error. This, however, can lead to large sectors and, in the case of a small number of antennas, this will lead to larger transformation errors and DOA estimation biases. The work at hand presents a novel pre-processing step used for sector discretization based on PCA and derives a novel concept from the UT [37].

The authors [38] proposed a novel nonlinear interpolation approach using MARS. The proposed approach is capable of interpolating arrays with a limited number of antennas and very distorted responses while keeping the DOA estimation bias low, heavily outperforming array linear interpolation methods. This performance improvement comes at the cost of increased computational cost. This work extends the MARS with advanced sector discretization methods that lead to a better performance and lower complexity. Furthermore, a more detailed mathematical description of the MARS method is presented. Expanding on the topic of nonlinear interpolation, the work at hand additionally presents a novel interpolation approach based on GRNNs. The proposed method is capable of achieving a performance similar to that of MARS in certain SNR regimes at a lower computational cost compared to the MARS based method.

In summary, this paper extends the concepts of array interpolation presented in previous research to explore the concepts of statistical significant sector discretization and nonlinear interpolation. Previous research focused on concepts for sector-by-sector processing, whereas this work aims to use a single unified sector discretized in a statistically significant manner. Moreover, this work develops novel nonlinear methods for array interpolation and presents a method suitable for real-time implementations capable of providing better performance than linear inter-

polation methods previously derived in the literature.

The results of the proposed discretization and interpolation methods are assessed via a set of studies considering measured responses obtained from a real physical system. The results show that all the proposed methods significantly improve DOA estimation considering a physical system and its inherent imperfections. Furthermore, this work analyzes the performance of the proposed interpolation methods when measurements of the true array response are not available and only simulated responses for building the interpolation models are available.

3. Data Model

This work considers a set of d wavefronts impinging onto a linear antenna array composed of M antennas. Figure 1 shows a graphical representation of the linear array. Considering the antenna elements are placed along the y -axis, the array geometry can be used to estimate the azimuth angle θ . For arrays composed of isotropic antennas, the elevation angle ϕ would have no influence on the antenna response, however, this work considers arrays with imperfect responses that have varying amplitude and phase responses of the different elements of the array with respect to the elevation angle of the received signals.

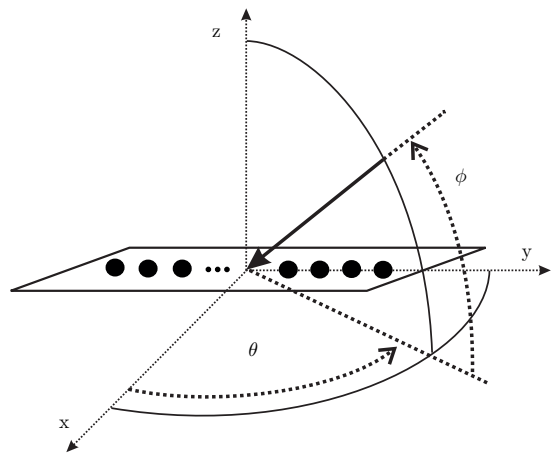


Figure 1: Graphical representation of a linear array

The received baseband signal at the array output can be expressed in matrix form as

$$\mathbf{X} = \mathbf{A}\mathbf{S} + \mathbf{N} \in \mathbb{C}^{M \times N}, \quad (1)$$

where $\mathbf{S} \in \mathbb{C}^{d \times N}$ is the matrix containing the N symbols transmitted by each of the d sources, $\mathbf{N} \in \mathbb{C}^{M \times N}$ is the noise matrix with its entries drawn from $\mathcal{CN}(0, \sigma_n^2)$, and

$$\mathbf{A} = [\mathbf{a}(\theta_1, \phi_1), \mathbf{a}(\theta_2, \phi_2), \dots, \mathbf{a}(\theta_d, \phi_d)] \in \mathbb{C}^{M \times d}, \quad (2)$$

where θ_i and ϕ_i are the azimuth and elevation angles of the i -th signal, and $\mathbf{a}(\theta_i, \phi_i) \in \mathbb{C}^{M \times 1}$ is the antenna array response.

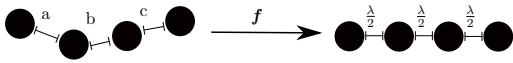


Figure 2: Example of array interpolation

The received signal covariance matrix $\mathbf{R}_{\mathbf{X}\mathbf{X}} \in \mathbb{C}^{M \times M}$ is given by

$$\mathbf{R}_{\mathbf{X}\mathbf{X}} = \mathbb{E}\{\mathbf{X}\mathbf{X}^{\text{H}}\} = \mathbf{A}\mathbf{R}_{\text{SS}}\mathbf{A}^{\text{H}} + \mathbf{R}_{\text{NN}}, \quad (3)$$

where $(\cdot)^{\text{H}}$ stands for the conjugate transpose, and

$$\mathbf{R}_{\text{SS}} = \begin{bmatrix} \sigma_1^2 & \gamma_{1,2}\sigma_1\sigma_2 & \cdots & \gamma_{1,d}\sigma_1\sigma_d \\ \gamma_{1,2}^*\sigma_1\sigma_2 & \sigma_2^2 & & \vdots \\ \vdots & & \ddots & \\ \gamma_{1,d}^*\sigma_1\sigma_d & \gamma_{2,d}^*\sigma_2\sigma_d & \cdots & \sigma_d^2 \end{bmatrix}, \quad (4)$$

where σ_i^2 is the power of the i -th signal and $\gamma_{i,i'} \in \mathbb{C}$, $|\gamma_{i,i'}| \leq 1$ is the cross-correlation coefficient between signals i and i' with $i \neq i'$. $\mathbf{R}_{\text{NN}} \in \mathbb{C}^{M \times M}$ the spatial covariance matrix of the noise. In case the entries of the noise matrix are drawn from $\mathcal{CN}(0, \sigma_n^2)$, $\mathbf{R}_{\text{NN}} = \mathbf{I}_M \sigma_n^2$, where \mathbf{I}_M denotes an $M \times M$ identity matrix. The Signal-to-Noise-Ratio (SNR) is defined as

$$\text{SNR} = \frac{\sigma_1^2}{\sigma_n^2} = \frac{\sigma_2^2}{\sigma_n^2} = \cdots = \frac{\sigma_d^2}{\sigma_n^2}. \quad (5)$$

An estimate of the received signal covariance matrix can be obtained by

$$\hat{\mathbf{R}}_{\mathbf{X}\mathbf{X}} = \frac{\mathbf{X}\mathbf{X}^{\text{H}}}{N} \in \mathbb{C}^{M \times M}. \quad (6)$$

4. Array Interpolation

Arrays can be interpolated by means of a one-to-one mapping given by

$$\mathbf{f} : \mathbf{A}_{\mathcal{S}} \rightarrow \bar{\mathbf{A}}_{\mathcal{S}}, \quad (7)$$

where \mathcal{S} is a sector. Figure 2 presents a graphical example of an array of arbitrary geometry being interpolated into a uniform linear array. Note that, even if an array has the required geometry for the usage of a certain array processing technique, its response may not adhere to an underlying assumed mathematical model. Therefore, in such cases, geometrically well behaved arrays may need to be interpolated to allow the application of the desired technique.

Definition 1. A sector \mathcal{S} is a finite and countable set of 2-tuples (pairs) of angles (θ, ϕ) containing all the combinations of azimuth and elevation angles representing a region of the field of view of the array. The sector \mathcal{S} defines the column space of $\mathbf{A}_{\mathcal{S}}$ and $\bar{\mathbf{A}}_{\mathcal{S}}$.

$\mathbf{A}_{\mathcal{S}} \in \mathbb{C}^{M \times |\mathcal{S}|}$ is the array response matrix formed out of the array response vectors $\mathbf{a}(\theta, \phi) \in \mathbb{C}^{M \times 1}$ of the angles given by the elements of \mathcal{S} . $\mathbf{A}_{\mathcal{S}}$ contains the true array response of the physical system, which may not possess important properties such as being centro-hermitian or Vandermonde. $\bar{\mathbf{A}}_{\mathcal{S}} \in \mathbb{C}^{M' \times |\mathcal{S}|}$ is the interpolated version of $\mathbf{A}_{\mathcal{S}}$ with columns $\bar{\mathbf{a}}(\theta, \phi) \in \mathbb{C}^{M' \times 1}$ being the array response of the so-called virtual or desired array, having all the properties necessary for posterior processing. $|\mathcal{S}|$ is the cardinality of the set \mathcal{S} , i.e. the number of elements in the set.

Definition 2. The mapping \mathbf{f} is said to be array size preserving if $M = M'$.

Definition 3. The mapping \mathbf{f} is said to be geometry preserving if it is size preserving and if the underlying array geometry for the true and virtual array is equivalent.

This work limits itself to mappings of linear planar arrays that are size and geometry preserving, as given in Definitions 2 and 3, respectively.

Linear array interpolation is usually done using a least squares approach. The problem is set up as finding a transformation matrix \mathbf{B} that is given by

$$\mathbf{B}\mathbf{A}_{\mathcal{S}} = \bar{\mathbf{A}}_{\mathcal{S}}, \quad (8)$$

The snapshot matrix \mathbf{X} can be transformed by multiplying it from the left-hand side with the transform matrix \mathbf{B} , which is equivalent to applying a linear model for each of the outputs of the virtual antenna array. Therefore, in linear array interpolation \mathbf{f} is given by the transformation matrix \mathbf{B} .

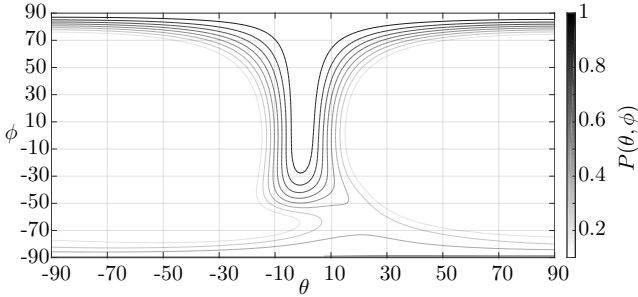
This model is usually not capable of transforming the response perfectly across the entire field of view except for the case where a large number of antenna elements is present or a very small sector is used. Large transformation errors often result in a large bias on the final DOA estimation, thus, usually, the response region is divided into a set of regions called sectors, and a different transform matrix is set up for each sector (sector-by-sector processing).

Nonlinear interpolation is an alternative to the linear approach capable of providing better accuracy under more challenging scenarios at the cost of increased complexity. In nonlinear interpolation, the mapping \mathbf{f} is given by a nonlinear function, such that

$$\mathbf{f}(v + \beta q) \neq \mathbf{f}(v) + \beta \mathbf{f}(q) \quad (9)$$

for some v , q and β .

Whatever array interpolation method is used, linear or nonlinear, the array response can only be interpolated after sector detection/selection and sector discretization. The following section presents a discussion on detection and selection of sectors of the field of view of the antenna array and how to discretize the detected sectors. Section 6 discusses nonlinear array interpolation methods in order

Figure 3: $P(\theta, \phi)$

to perform a one-to-one mapping between the true and the virtual array response considering the discretized sectors. Section 6 details the process of nonlinear interpolation presenting two distinct methods.

5. Sector Selection and Discretization

Traditionally, the field of view of the array is divided into sectors that are small enough to keep the interpolation bias bounded. These sectors can be made larger or smaller depending on the accuracy desired for the interpolation. After the field of view is divided the sectors are discretized uniformly using a fine grid and sector-by-sector interpolation is performed.

To avoid performing sector-by-sector interpolation this work uses a single combined sector containing all regions of the field of view of the array where significant power is received. Considering that the response of the true array needs to be known to construct a transformation of the interpolation of the received signal, this response can be used to detect angular regions where significant power is received in order to detect sectors adaptively. To this end, the conventional beamformer [39] can be applied to provide an estimate of angular regions where significant power is received. The beamformer yields the normalized power response

$$P(\theta, \phi) = \frac{\mathbf{a}^H(\theta, \phi) \hat{\mathbf{R}}_{\mathbf{X}\mathbf{X}} \mathbf{a}(\theta, \phi)}{\mathbf{a}^H(\theta, \phi) \mathbf{a}(\theta, \phi)} \in \mathbb{R}. \quad (10)$$

Figure 3 shows an example of the real data output of (10) for a signal received at the six element linear physical antenna array shown in Figure 7 with $\theta = 0^\circ$, $\phi = 20^\circ$, SNR = 30 dB, and $N = 10$.

In physical systems, the result of (10) is discrete in θ and ϕ , and can be written as

$$P[z, v] = P(-90^\circ + (z \cdot \Delta_\theta), -90^\circ + (v \cdot \Delta_\phi)) = P(\theta, \phi), \quad (11)$$

with $z \in \mathbb{N}_0$, $v \in \mathbb{N}_0$, $\theta \in \mathcal{D}_{\Delta_\theta}$, and $\phi \in \mathcal{D}_{\Delta_\phi}$ where

$$\mathcal{D}_{\Delta_\theta} = \{-90^\circ, -90^\circ + \Delta_\theta, \dots, 90^\circ - \Delta_\theta, 90^\circ\}, \quad (12)$$

$$\mathcal{D}_{\Delta_\phi} = \{-90^\circ, -90^\circ + \Delta_\phi, \dots, 90^\circ - \Delta_\phi, 90^\circ\}. \quad (13)$$

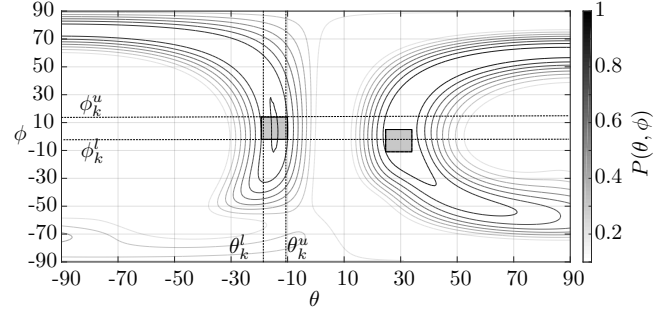


Figure 4: Selected sectors and example of sector bounds

Here, $\Delta_\theta \in \mathbb{R}^+$ and $\Delta_\phi \in \mathbb{R}^+$ are the resolution of the azimuth and elevation angles of the power response (10), respectively.

Figure 4 presents an example of the real data output of (11) when two signals are transmitted from $(-5^\circ, 0^\circ)$ and $(30^\circ, -10^\circ)$, with SNR = 30 dB, and $N = 10$ at the physical array shown in Figure 7. This normalized power response is scanned for sectors \mathcal{S}_k , and for each sector, the respective lower bounds $\theta_k^l \in \mathcal{D}_{\Delta_\theta}$ and $\phi_k^l \in \mathcal{D}_{\Delta_\phi}$, as well as the upper bounds $\theta_k^u \in \mathcal{D}_{\Delta_\theta}$ and $\phi_k^u \in \mathcal{D}_{\Delta_\phi}$ are defined as shown in Figure 4. A threshold $\alpha\sigma_n^2$, with $\alpha \in \mathbb{R}^+$, defines a sector \mathcal{S}_k considering the criterion $P(\theta, \phi) \geq \alpha\sigma_n^2$ and $k = 1, \dots, K$. A sector can be defined as

$$\mathcal{S}_k = \Theta_k \times \Phi_k = \{(\theta, \phi) | \theta \in \Theta_k \wedge \phi \in \Phi_k\}, \quad (14)$$

where

$$\Theta_k = \{\theta | \theta_k^l \leq \theta \leq \theta_k^u\} \subseteq \mathcal{D}_{\Delta_\theta}, \quad (15)$$

$$\Phi_k = \{\phi | \phi_k^l \leq \phi \leq \phi_k^u\} \subseteq \mathcal{D}_{\Delta_\phi}, \quad (16)$$

and

$$\forall_{\substack{K \\ k, k' = 1 \\ k \neq k'}} \mathcal{S}_k \cap \mathcal{S}_{k'} = \emptyset. \quad (17)$$

A combined sector can be defined as

$$\mathcal{S} = \mathcal{S}_1 \cup \dots \cup \mathcal{S}_k \cup \dots \cup \mathcal{S}_K \subseteq \mathcal{D}_{\Delta_\theta} \times \mathcal{D}_{\Delta_\phi}. \quad (18)$$

Most array signal processing techniques assume the presence of isotropic elements. However, in reality, the responses of antennas are never isotropic. Therefore, even for linear arrays, the sectors have to be built taking into account the elevation angle in order to obtain an accurate interpolation. However, for most linear antenna arrays with non-isotropic element responses, the resolution with which the elevation angle ϕ can be estimated is expected to be very low (assuming isotropic elements it is not possible at all). Furthermore, for elevation angles close to zenith, i.e. $\phi \approx 90^\circ$, the angular resolution in azimuth is decreased. This is expected even for arrays composed of perfectly isotropic antennas as there will be no phase

difference for different azimuth angles when elevation angles are close to zenith. This is shown in Figure 3. The fact that there is a low angular resolution in elevation implies that the response of the array is not heavily affected by changes in elevation angle. Therefore, choosing a fixed elevation angle for the interpolation of a sector is often sufficient if the chosen elevation angle is sufficiently close to the elevation angle of the received signal.

The proposed sector detection and selection technique can be directly applied to two-dimensional arrays such as uniform rectangular arrays (URAs). For such arrays, the elevation estimation will have a greatly improved resolution. Moreover, for such arrays, it will often be beneficial to interpolate the response in elevation to allow high-resolution techniques to be applied.

Within each of the detected sectors \mathcal{S}_k several nearly coherent and closely-spaced signals could be received. Since these signals are represented by similar array responses, an interpolation considering this sector is efficient for all received signals. After interpolation, such signals can be separated with techniques such as SPS and FBA, allowing the application of a high-resolution DOA estimation method to jointly estimate the parameters of all the detected signals. Thus, the separation of closely-spaced sources is only limited by the high-resolution DOA estimation method and by the number of elements of the antenna array, but not by the array interpolation itself.

To address cases where the noise floor is high a large α can be used. However, this means that only large sectors are detected, at the cost of discarding smaller sectors that are related to a signal component. On the other hand, smaller α means that smaller sectors are detected but at the cost of allowing noise to be mistakenly detected as a sector. Selecting noise regions as sectors will result in a smaller estimation bias than leaving regions with signal power out of the transform. Therefore, for cases where the noise floor is high compared to the signal strength, an α that sets the cutoff to be close to the noise floor is recommended.

For arrays where the response does not vary strongly with elevation, or for setups where signals are received by the array at a given narrow set of elevation angles, ϕ can be fixed. Thus, the output of (10) becomes one-dimensional, and the sector selection shown in Figure 4 can be simplified to a one-dimensional problem as shown in Figure 5.

In this case, the sectors \mathcal{S}_k are defined only by their lower and upper bounds θ_k^l and θ_k^u respectively. Previous works on array interpolation created a discrete uniform set of angles within each sector. Instead of using uniform sector discretization, the next subsections present two different methods for sector discretization aiming to preserve the statistical properties of the considered sectors \mathcal{S}_k .

5.1. UT Discretization

The UT [23] is a transformation used to transform a continuous probability density function (PDF) into a discrete probability mass function (PMF). The UT can be

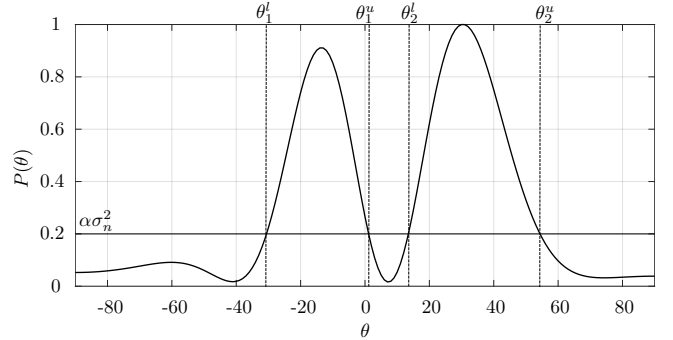


Figure 5: Selected sectors and respective bounds for one-dimensional case

applied in array interpolation to discretize the detected sectors in such a way that the statistical properties, the moments, of the detected sectors are preserved in its discrete form. Thus, no statistical information is lost, since a PDF can be fully represented by its moments as stated in the following theorem.

Theorem 1. *A probability density function can be entirely described by its moments.*

Proof. A proof can be found in Appendix A. \square

The UT discretization can be applied by solving the nonlinear set of equations

$$\sum_{j=1}^{k-1} w_j S_j^k = w_1 S_1^k + \dots + w_{k-1} S_{k-1}^k = \mathbb{E}\{r^k\}. \quad (19)$$

where S_j are known as sigma points, w_j are its respective weights, and r is the value assumed by a continuous random variable \tilde{r} . From (19) it is clear that in order to preserve the characteristics of \tilde{r} up to the k -th moment, it is necessary to calculate $k-1$ sigma points and its weights by solving a nonlinear system of equations. Thus, there is a trade-off between simplicity in the calculation and the accuracy of the representation of higher order moments.

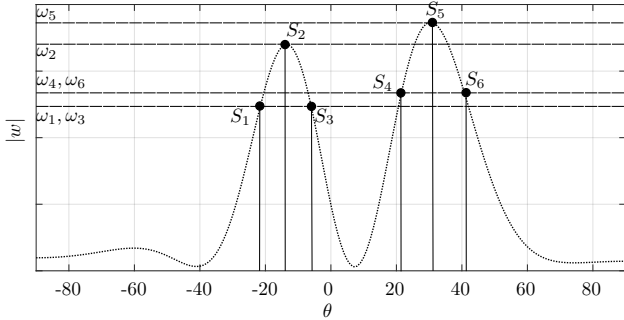
The UT can be applied to an approximation of the concentrated loss function $l_c(\mathbf{X}; \boldsymbol{\theta}, \boldsymbol{\phi})$ and thus the log-likelihood $l(\mathbf{X}; \boldsymbol{\theta}, \boldsymbol{\phi})$ of the DOA estimation problem, which is derived in the following theorem. The concentrated loss function $l_c(\mathbf{X}; \boldsymbol{\theta}, \boldsymbol{\phi})$ and the log-likelihood $l(\mathbf{X}; \boldsymbol{\theta}, \boldsymbol{\phi})$ of the DOA estimation problem at hand are defined in (B.1) and (B.4), and

$$\boldsymbol{\theta} = [\theta_1, \dots, \theta_d]^T, \quad (20)$$

$$\boldsymbol{\phi} = [\phi_1, \dots, \phi_d]^T. \quad (21)$$

Theorem 2. *The concentrated loss function $l_c(\mathbf{X}; \boldsymbol{\theta}, \boldsymbol{\phi})$ for a DOA estimation problem can be approximated for each detected sector \mathcal{S}_k by the normalized power response of the conventional beamformer (10).*

Proof. A proof can be found in Appendix B. \square

Figure 6: UT of the approximated $l_c(\mathbf{X}; \boldsymbol{\theta}, \phi)$ for two sources

Following the approximation derived in Theorem 2 the concentrated loss function and thus the log-likelihood with respect to each sector \mathcal{S}_k can be considered as a separate PDF each when applying the UT. In order to preserve the first and the second moment of the approximated log-likelihood, the number of points are chosen to transform each detected sector \mathcal{S}_k must be larger or equal than 3. Under this constraint and under the assumption that the input noise follows $\mathcal{CN}(0, \sigma_n^2)$, the respective PDF characteristics for each sector \mathcal{S}_k are mainly preserved. Figure 6 presents how the concentrated loss function $l_c(\mathbf{X}; \boldsymbol{\theta}, \phi)$ can be represented using the UT for a linear array assuming uniform antenna responses of the different antennas in elevation. A total transformation sector by concatenating all the sigma points given by the UT for the detected sectors can be written as

$$\mathbf{A}_{\mathcal{S}} = [\mathbf{a}(S_1), \mathbf{a}(S_2), \dots, \mathbf{a}(S_T)] \in \mathbb{C}^{M \times T}, \quad (22)$$

where T is the total number of points used to discretize all the detected sectors.

The proposed UT-based discretization is well suited for linear arrays that have a uniform response in elevation. The calculation of the sigma points S_t and weights ω_t with $t = 1, \dots, T$ of the UT transformation is computationally expensive. Therefore, calculating multiple sets of points across multiple elevations may become infeasible depending on the application and system at hand. The UT can be very useful also when applying linear interpolation, as it can be used to ensure that the least squares calculation of the transformation matrix is a determined problem instead of an overdetermined one.

5.2. Principal Component Discretization

For most interpolation methods presented in the literature, the interpolated sectors are discretized using a simple uniform discretization. The discretization is usually done such that the discrete angles are closely spaced. Therefore, the steering vectors of such closely spaced angles are highly correlated. This work proposes the application of principal component analysis (PCA) to avoid problems caused by the correlation in predictors as well as to minimize the computational load of the transformation.

Ideally, $\mathbf{A}_{\mathcal{S}}$ would be set up such that $\mathbf{A}_{\mathcal{S}}\mathbf{A}_{\mathcal{S}}^H = \mathbf{I}_M$. However, as stated previously, this is often not the case with $\mathbf{A}_{\mathcal{S}}\mathbf{A}_{\mathcal{S}}^H = \mathbf{R}_{\mathbf{A}_{\mathcal{S}}\mathbf{A}_{\mathcal{S}}} \neq \mathbf{I}_M$. PCA aims to find a matrix \mathbf{P} such that

$$\mathbf{P}\mathbf{A}_{\mathcal{S}} = \mathbf{B}_{\mathcal{S}}, \quad (23)$$

where $\mathbf{B}_{\mathcal{S}}\mathbf{B}_{\mathcal{S}}^H = \mathbf{I}_M$. \mathbf{P} can be obtained by performing the eigendecomposition of $\mathbf{R}_{\mathbf{A}_{\mathcal{S}}\mathbf{A}_{\mathcal{S}}}$

$$\mathbf{R}_{\mathbf{A}_{\mathcal{S}}\mathbf{A}_{\mathcal{S}}} = \mathbf{E}\boldsymbol{\Sigma}\mathbf{E}^H, \quad (24)$$

and setting $\mathbf{P} = \mathbf{E}$. The proposed PCA pre-processing can be used to create a better set of predictor variables for the interpolation and to reduce the dimensionality of the problem by excluding any eigenvectors associated to very small eigenvalues.

6. Nonlinear Interpolation

In this section two independent nonlinear alternatives to array interpolation, allowing the application of FBA and SPS in highly correlated signal scenarios, are presented. Subsection 6.1 presents an interpolation approach based on the MARS regression method, allowing a model to be created expressing nonlinear relationships between the true and the desired array response. Subsection 6.2 shows an interpolation approach based on GRNNs, this approach can be implemented in a parallel manner, making it a good candidate for array interpolation under real-time constraints.

6.1. MARS Based Interpolation

This work proposes a nonlinear interpolation method based on the MARS technique [24]. The proposed interpolation approach builds an augmented mapping that splits the real and imaginary parts of the response of each of the antennas of the array, that is, a total of $2M$ MARS models are built to interpolate the array response with respect to the combined sector \mathcal{S} . This mapping can be written as

$$\forall (\boldsymbol{\theta}, \phi) \in \mathcal{S} : \begin{bmatrix} \Re\{\bar{\mathbf{a}}(\boldsymbol{\theta}, \phi)\} \\ \Im\{\bar{\mathbf{a}}(\boldsymbol{\theta}, \phi)\} \end{bmatrix} = \mathbf{f}(\mathbf{a}(\boldsymbol{\theta}, \phi))$$

$$= \begin{bmatrix} \sum_{\ell=1}^{L_1^R} c_{\ell,1}^R F_{\ell,1}^R (\Re\{\mathbf{a}(\boldsymbol{\theta}, \phi)\}) \\ \vdots \\ \sum_{\ell=1}^{L_M^R} c_{\ell,M}^R F_{\ell,M}^R (\Re\{\mathbf{a}(\boldsymbol{\theta}, \phi)\}) \\ \sum_{\ell=1}^{L_1^I} c_{\ell,1}^I F_{\ell,1}^I (\Im\{\mathbf{a}(\boldsymbol{\theta}, \phi)\}) \\ \vdots \\ \sum_{\ell=1}^{L_M^I} c_{\ell,M}^I F_{\ell,M}^I (\Im\{\mathbf{a}(\boldsymbol{\theta}, \phi)\}) \end{bmatrix}, \quad (25)$$

where $c_{l_m}^R$ and $c_{l_m}^I$ are the weighting constants, $F_{l_m}^R$ and $F_{l_m}^I$ are the basis functions and L_m^R and L_m^I are the number of functions and weighting constants of each model. Furthermore, $\Re\{\bar{\mathbf{a}}(\boldsymbol{\theta}, \phi)\}$ and $\Im\{\bar{\mathbf{a}}(\boldsymbol{\theta}, \phi)\}$ denote the real and imaginary part of vector $\bar{\mathbf{a}}(\boldsymbol{\theta}, \phi)$, respectively. The

basis functions F_m^R and F_m^I are hinge functions or multiplications of hinge functions [24]. The original generalized cross-validation (GCV) for the backward pass used in MARS can be reformulated considering the array interpolation problem as

$$\Re\{\text{GCV}\} = \frac{\frac{1}{|\mathcal{S}|} \sum_{(\theta, \phi) \in \mathcal{S}} (\Re\{\bar{\mathbf{a}}_{[m]}(\theta, \phi)\} - \mathbf{f}_m^R(\mathbf{a}(\theta, \phi)))^2}{\left(1 - \frac{L_m^R + p \frac{L_m^R - 1}{2}}{|\mathcal{S}|}\right)^2}, \quad (26)$$

$$\Im\{\text{GCV}\} = \frac{\frac{1}{|\mathcal{S}|} \sum_{(\theta, \phi) \in \mathcal{S}} (\Im\{\bar{\mathbf{a}}_{[m]}(\theta, \phi)\} - \mathbf{f}_m^I(\mathbf{a}(\theta, \phi)))^2}{\left(1 - \frac{L_m^I + p \frac{L_m^I - 1}{2}}{|\mathcal{S}|}\right)^2}, \quad (27)$$

where \mathbf{f}_m^R and \mathbf{f}_m^I are the real and imaginary part of the model for the m -th antenna, respectively. Both $\Re\{\text{GCV}\}$ and $\Im\{\text{GCV}\}$ are used to avoid over-fitting, that is, to reduce the complexity of the model created in order to avoid fitting of the noise or of measurement errors of the array response. $\bar{\mathbf{a}}_{[m]}(\theta, \phi)$ denotes the m -th element of the virtual array response. To use this approach in an online system the models can be built in an initialization step. Sectors of interest for the application of the MARS interpolation can be selected and a model can be built and stored as a look-up table. The data received can be interpolated snapshot-wise with

$$\begin{bmatrix} \Re\{\bar{\mathbf{x}}[n]\} \\ \Im\{\bar{\mathbf{x}}[n]\} \end{bmatrix} = \mathbf{f}(\mathbf{x}[n]), \quad (28)$$

where $\mathbf{x}[n] \in \mathbb{C}^{M \times 1}$ is the n -th column of matrix \mathbf{X} with $n = 1, \dots, N$.

In some cases, the antenna array will have a response which is similar enough to the desired response in some of its field of view so that a linear approach yields good results. Thus, the MARS approach can be used only on portions of the field of view where the true response differs strongly from the desired one.

The MARS approach is especially useful for arrays with a small number of elements. For linear approaches, the degrees of freedom of the linear approach are limited by the number of antennas in the virtual array. It is possible to increase the degrees of freedom by creating a virtual array with a larger number of antennas, however, this will lead to a transformation matrix that is ill-conditioned and results in a large bias in the DOA estimates. The MARS approach, on the other hand, can build as many hinge functions and relationships between them as necessary. While MARS will still benefit from having a larger array, since it provides more input variables for the model, it is less sensitive to a reduction in the size of the array.

6.2. GRNN Based Interpolation

GRNNs [25] are a type of neural network used for general regression problems that are extended in this work for the problem of array interpolation.

Classic interpolation relies on transforming an array response over the discrete set of angles \mathcal{S} . In linear array

interpolation, the choice of points that belong to \mathcal{S} is usually an arbitrary one, based solely on the predefined sector bounds and the chosen angular resolution. When applying a linear approach, angular resolution is usually chosen to be as high as possible, thus, the set of points belonging to \mathcal{S} is usually closely spaced. This is not necessary when applying the GRNN since it is capable of interpolating between multiple sets of training data. In fact, a dense set of training points will result in an increased computational load while providing very little benefit to the overall accuracy of the GRNN based array interpolation.

The neural network representing the real and imaginary parts of the array can be built by extending the original structure of GRNNs to the application at hand, resulting in the mapping

$$\begin{bmatrix} \Re\{\bar{\mathbf{x}}[n]\} \\ \Im\{\bar{\mathbf{x}}[n]\} \end{bmatrix} = \mathbf{f}(\mathbf{x}[n], \bar{\mathbf{a}}(\theta, \phi), \mathbf{a}(\theta, \phi)), \quad (29)$$

and

$$\Re\{\bar{\mathbf{x}}_{[m]}[n]\} = \frac{\sum_{(\theta, \phi) \in \mathcal{S}} \Re\{\bar{\mathbf{a}}_{[m]}(\theta, \phi)\} e^{-\frac{\xi(\theta, \phi)}{2\sigma^2}}}{\sum_{(\theta, \phi) \in \mathcal{S}} e^{-\frac{\xi(\theta, \phi)}{2\sigma^2}}}, \quad (30)$$

$$\Im\{\bar{\mathbf{x}}_{[m]}[n]\} = \frac{\sum_{(\theta, \phi) \in \mathcal{S}} \Im\{\bar{\mathbf{a}}_{[m]}(\theta, \phi)\} e^{-\frac{\xi(\theta, \phi)}{2\sigma^2}}}{\sum_{(\theta, \phi) \in \mathcal{S}} e^{-\frac{\xi(\theta, \phi)}{2\sigma^2}}}, \quad (31)$$

where σ^2 is the smoothness parameter, and

$$\xi(\theta, \phi) = \|\mathbf{x}[n] - \mathbf{a}(\theta, \phi)\|_2^2. \quad (32)$$

Once the data has been interpolated to the desired array structure, array signal processing schemes such as FBA, SPS or ESPRIT can be applied.

Linear interpolation methods and the MARS method, as shown in (28), are direct functions of the received signal plus noise at the input of the array. Therefore, these methods have noise coloring as a side effect that needs to be taken into account when performing DOA estimation. On the other hand, there is no noise color introduced by the GRNN based interpolation, therefore pre-whitening is not necessary. This can be observed by considering (30) and (31) which are a sum of the desired ideal response vectors weighted by the similarity between the received signal and its respective true response vector counterpart. Thus, using the GRNN method, a larger noise level will lead to the interpolation being steered away from the real direction from where the signal is received. Thus, the output of the interpolation can be seen as noiseless, but not error free, as the noise present in the original data induces interpolation errors that will lead to a bias in the final DOA estimation.

One of the advantages of applying GRNNs to array interpolation is that the sectors considered for transformation can be made very large while having a small effect on the accuracy of the interpolation. As shown in (30, 31),

in case the input resembles the data used for the training in a certain region of the transformed sector, this data will have a larger weight. On the other hand, if the input is distant from any region of the transformed sector, this region will have very little influence on the output of the interpolation.

Therefore, with a GRNN it is possible to transform very large regions of the field of view of the array without suffering from the same problems as the ones present in linear array interpolation, where the transformation error grows as the transformed region grows. On the other hand, transforming a large region using the GRNN will increase the computational cost of the interpolation. Due to the parallelizable structure of GRNNs, it is possible to implement the proposed GRNN array interpolation in a parallel manner, leading to a faster interpolation. Thus, the proposed GRNN array interpolation is a possible alternative for precise array interpolation in real time applications.

7. Numerical Simulations

The performance of the proposed algorithms is tested considering a manufactured 6×1 linear antenna array shown in Figure 7. The single antennas are circularly polarized dielectric resonator antennas (DRA) [40], exhibiting a strong miniaturization of the aperture. The antennas are tuned to work at GPS L1 frequency band centered around 1575.42 MHz in standalone configuration. Once in the array, no attempt has been made to re-tune them, in order to emphasize the mutual coupling effects and eventual degradation. This 6×1 linear array was especially designed for research on mutual coupling with adjustable inter-element spacing of the 6 antennas. The small dimensions of the single antennas allow to place them quite close to each other, up to a minimum distance of 30 mm ($\approx 0.16\lambda$ at L1 central frequency). The following simulations consider array responses of the manufactured array measured in an anechoic chamber as well as array responses simulated using a 3D electromagnetic simulator (ANSYS HFSS). Thus, realistic assessment of the proposed algorithms can be achieved considering measured and properly simulated array responses.

The simulations are performed considering the receiver has no previous knowledge of the received signal. The combined sector is detected and discretized according to the methods presented in Section 5. After discretization the combined sector is interpolated using the methods proposed in Section 6. The model order of the interpolated data then is estimated by applying FBA and SPS adaptively and using RADOI [10] as the model order estimation method following the procedure proposed in [35]. Once model order is estimated the DOA estimates are obtained using TLS-ESPRIT [6].

For obtaining $\hat{\mathbf{R}}_{\mathbf{X}\mathbf{X}}$ $N = 100$ snapshots are used and the Root Mean Squared Error (RMSE) is calculated with respect to 1000 Monte Carlo simulations. Two signals from $\theta_1 = 45^\circ$ and $\theta_2 = 15^\circ$ with $\sigma_1^2 = \sigma_2^2 = 1$ and $\gamma_{1,2} = 1$

according to (4) are impinging on the array. The given RMSE is

$$\text{RMSE} = \sqrt{\frac{1}{K} \sum_{k=1}^K \left((\hat{\theta}_1^k - \theta_1)^2 + (\hat{\theta}_2^k - \theta_2)^2 \right)}, \quad (33)$$

where $\hat{\theta}_i^k$ is the estimate of θ_i at the k -th Monte Carlo run.

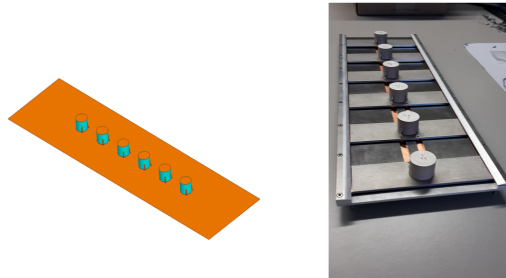
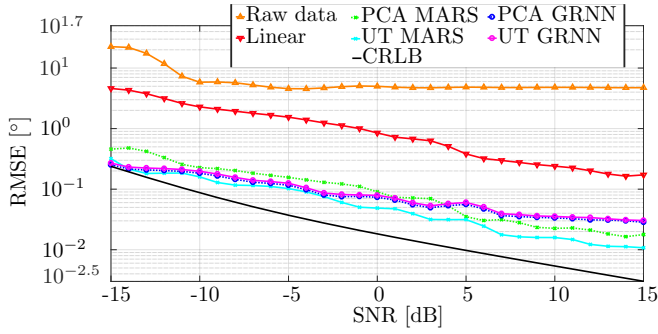


Figure 7: 6×1 antenna array: ANSYS HFSS model (left), prototype (right).

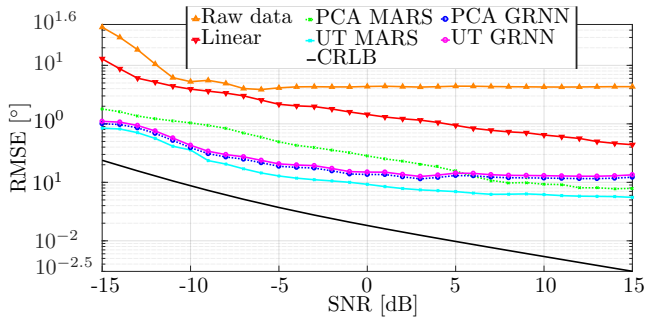
7.1. Performance of Proposed Methods With Measured Array Response Knowledge

The first set of simulations studies the performance of the proposed methods using the measured array response to build the interpolation models. Figure 8 presents the performance of the discretization and interpolation methods proposed in this work when the array is measured with 0.4λ inter-element spacing. As a benchmark, the results achieved with no interpolation, denoted as raw data in the figures, with the linear interpolation approach from [35], and the Cramér–Rao lower bound (CRLB) [14] are presented. The results show that, if no interpolation is applied, a constant bias is present for the DOA estimates even at high SNRs. The linear approach is capable of providing a DOA estimation accuracy superior to one degree at positive SNRs. The proposed nonlinear approaches offer greatly improved performance when compared to the linear approach. The MARS approach is shown to benefit significantly from the UT discretization. This is expected as the UT discretization reduces the overall complexity and possible over-fitting of the MARS model, as the mapping needs to consider only the statistically significant regions of the sector. The proposed GRNN approach is shown to have a very similar performance when either PCA or the UT are used as a discretization method. As the computational complexity of the PCA-based discretization method is significantly smaller than that of the UT-based method, PCA becomes more attractive when the GRNN method is used for interpolation.

In the second set of simulations, presented in Figure 9, the inter-element spacing between is set to 0.2λ . In this configuration the mutual coupling between antenna elements is very strong and the radiation patterns are highly

Figure 8: DOA estimation performance with 0.4λ element separation

distorted when compared to isotropic patterns. The difference in performance between the proposed nonlinear methods and the bench mark linear method becomes more significant when compared to the 0.4λ inter-element spacing. The challenging scenario also highlights the performance difference between the proposed discretization and interpolation methods. The performance of the MARS based method with the UT pre-processing significantly outperforms its PCA variant.

Figure 9: DOA estimation performance with 0.2λ element separation

7.2. Performance of Proposed Methods With Simulated Array Response Knowledge

Obtaining the response of an antenna over its entire field of view with a fine enough resolution for performing array interpolation requires a well equipped anechoic chamber. In case such a chamber is not available, the interpolation can be done using a properly simulated array response. With the next set of simulations the performance of the proposed methods if the array response that is considered by the algorithms is not the true (measured) array response but is derived from simulations using a 3D electromagnetic simulator (ANSYS HFSS) is studied. The results shown in Figure 10 were obtained by setting the inter-element spacing of the antennas to 0.4λ . The simulation results of the array interpolation methods show that the performance of all methods is degraded by the imperfect knowledge of the array response (simulated array response). Despite the decrease in performance, the proposed methods are capable of achieving an accuracy of a tenth of a degree for moderate SNRs.

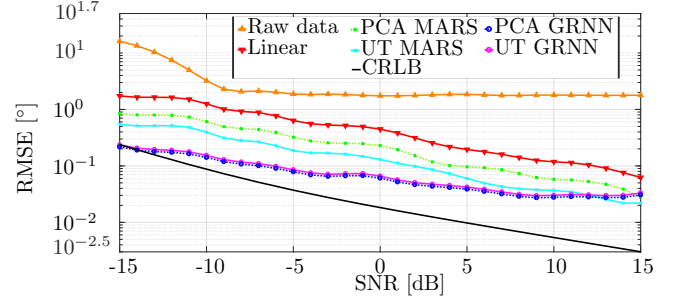
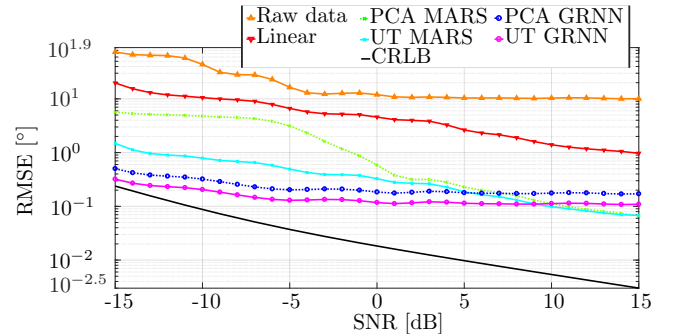
Figure 10: DOA estimation performance for model built with simulated data with 0.4λ element separation

Figure 11 presents the results of the simulations when the inter-element is 0.2λ and the model is built using a simulated array response. In this case the proposed PCA approaches suffer heavy degradation. This is due to the fact that the principal components of the simulated array response do not represent the principal components of the true array response (measured array response) well enough for building a proper model. In this scenario the linear approach is not capable of providing an accuracy below one degree.

Figure 11: DOA estimation performance for model built with simulated data with 0.2λ element separation

7.3. Failure Rate Performance

In the last set of simulations the failure rate of the TLS-ESPRIT used for DOA estimation is studied. For this simulation a single signal is received by the array with $\theta = 80^\circ$ and the array has an inter-element spacing of 0.2λ . Figure 12 compares the failure rates of non-interpolated data with interpolated data using the UT-based discretization and the MARS method. For these simulations TLS-ESPRIT is considered to fail if the eigendecomposition of the solution for the shift invariance equation of TLS-ESPRIT yields complex eigenvalues. The simulations show that the proposed interpolation method is capable of significantly reducing the failure rate of subspace based methods for regions near end-fire of the array.

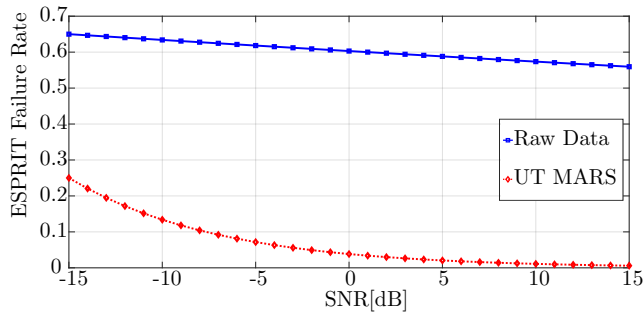


Figure 12: TLS-ESPRIT failure rate for 0.2λ element separation

8. Conclusions

In this work two novel discretization methods based on the UT and PCA were presented. The UT-based method is capable of discretizing the detected sectors while preserving their statistical properties. Due to the computational complexity involved this method is best suited for arrays with a small number of elements. The PCA-based method is best suited for arrays with a large number of elements, as it can be used to reduce the dimensionality of the problem resulting in a lower computational load.

Additionally, two novel nonlinear interpolation methods were presented which are derived from nonlinear regression methods, MARS and GRNNs. The MARS interpolation can be calculated offline, allowing it to be used in real time systems in cases where the signals are expected to come from a limited region of the field of view of the array and is capable of achieving good performance at moderate to high SNRs. The GRNN-based approach has reduced computational complexity compared to the MARS due to the high degree of parallelization of the method and provides a better performance for low SNRs.

Acknowledgments

The research leading to the results reported in this paper has received funding from Coordenação de Aperfeiçoamento de Pessoal de Nível Superior (CAPES) under the PVE grant number 88881.030392/2013-01 and by the EL-LIIT Strategic Research Network. This support is greatly acknowledged.

- [1] E. G. Larsson, O. Edfors, F. Tufvesson, T. L. Marzetta, Massive mimo for next generation wireless systems, *IEEE Communications Magazine* 52 (2) (2014) 186–195.
- [2] T. Virtanen, Monaural sound source separation by nonnegative matrix factorization with temporal continuity and sparseness criteria, *IEEE transactions on audio, speech, and language processing* 15 (3) (2007) 1066–1074.
- [3] Y. Bresler, A. Macovski, Exact maximum likelihood estimation of superimposed exponential signals in noise 10 (1985) 1824–1827.

- [4] P. Stoica, K. C. Sharman, Novel eigenanalysis method for direction estimation, in: *IEE Proceedings F (Radar and Signal Processing)*, Vol. 137, IET, 1990, pp. 19–26.
- [5] A. Barabell, Improving the resolution performance of eigenstructure-based direction-finding algorithms, in: *Acoustics, Speech, and Signal Processing, IEEE International Conference on ICASSP'83.*, Vol. 8, IEEE, 1983, pp. 336–339.
- [6] R. Roy, T. Kailath, ESPRIT-estimation of signal parameters via rotational invariance techniques, *IEEE Transactions on acoustics, speech, and signal processing* 37 (7) (1989) 984–995.
- [7] J. E. Evans, J. R. Johnson, D. Sun, Application of advanced signal processing techniques to angle of arrival estimation in ac navigation and surveillance systems, Tech. rep., Lincoln Laboratory (1982).
- [8] S. U. Pillai, B. H. Kwon, Forward/backward spatial smoothing techniques for coherent signal identification, *IEEE Transactions on Acoustics, Speech, and Signal Processing* 37 (1) (1989) 8–15.
- [9] M. Wax, T. Kailath, Detection of signals by information theoretic criteria, *IEEE Transactions on Acoustics, Speech, and Signal Processing* 33 (2) (1985) 387–392.
- [10] E. Radoi, A. Quinquis, A new method for estimating the number of harmonic components in noise with application in high resolution radar, *EURASIP Journal on Advances in Signal Processing* 2004 (8) (2004) 1177–1188.
- [11] J. P. C. da Costa, M. Haardt, F. Romer, G. Del Galdo, Enhanced model order estimation using higher-order arrays (2007) 412–416.
- [12] J. P. C. L. da Costa, F. Roemer, M. Haardt, R. T. de Sousa, Multi-dimensional model order selection, *EURASIP Journal on Advances in Signal Processing* 2011 (1) (2011) 26.
- [13] B. Ottersten, M. Viberg, T. Kailath, Analysis of subspace fitting and ml techniques for parameter estimation from sensor array data, *IEEE Transactions on Signal Processing* 40 (3) (1992) 590–600.
- [14] B. Ottersten, M. Viberg, P. Stoica, A. Nehorai, Exact and large sample maximum likelihood techniques for parameter estimation and detection in array processing, in: *Radar array processing*, Springer, 1993, pp. 99–151.
- [15] A. P. Dempster, N. M. Laird, D. B. Rubin, Maximum likelihood from incomplete data via the em algorithm, *Journal of the royal statistical society. Series B (methodological)* (1977) 1–38.
- [16] T. K. Moon, The expectation-maximization algorithm, *IEEE Signal processing magazine* 13 (6) (1996) 47–60.
- [17] M. I. Miller, D. R. Fuhrmann, Maximum-likelihood narrow-band direction finding and the em algorithm, *IEEE Transactions on Acoustics, Speech, and Signal Processing* 38 (9) (1990) 1560–1577.
- [18] J. A. Fessler, A. O. Hero, Space-alternating generalized expectation-maximization algorithm, *IEEE Transactions on Signal Processing* 42 (10) (1994) 2664–2677.
- [19] F. A. Dietrich, A tutorial on channel estimation with sage.
- [20] F. Antreich, J. A. Nossek, G. Seco-Granados, A. L. Swindlehurst, The extended invariance principle for signal parameter estimation in an unknown spatial field, *IEEE Transactions on Signal Processing* 59 (7) (2011) 3213–3225.
- [21] M. Buhren, M. Pesavento, J. F. Bohme, Virtual array design for array interpolation using differential geometry, in: *Acoustics, Speech, and Signal Processing, 2004. Proceedings. (ICASSP'04). IEEE International Conference on*, Vol. 2, IEEE, 2004, pp. ii–229.
- [22] B. Friedlander, The root-music algorithm for direction finding with interpolated arrays, *Signal Processing* 30 (1) (1993) 15–29.
- [23] S. J. Julier, J. K. Uhlmann, A new extension of the kalman filter to nonlinear systems, in: *Int. symp. aerospace/defense sensing, simul. and controls*, Vol. 3, Orlando, FL, 1997, pp. 182–193.
- [24] J. H. Friedman, Multivariate adaptive regression splines, *The annals of statistics* (1991) 1–67.
- [25] D. F. Specht, A general regression neural network, *IEEE transactions on neural networks* 2 (6) (1991) 568–576.
- [26] T. P. Bronez, Sector interpolation of non-uniform arrays for efficient high resolution bearing estimation, in: *Acoustics, Speech,*

- and Signal Processing, 1988. ICASSP-88., 1988 International Conference on, IEEE, 1988, pp. 2885–2888.
- [27] B. Friedlander, A. J. Weiss, Direction finding using spatial smoothing with interpolated arrays, *IEEE Transactions on Aerospace and Electronic Systems* 28 (2) (1992) 574–587.
- [28] M. Buhren, M. Pesavento, J. Bohme, A new approach to array interpolation by generation of artificial shift invariances: interpolated esprit, in: *Acoustics, Speech, and Signal Processing, 2003. Proceedings.(ICASSP'03). 2003 IEEE International Conference on, Vol. 5, IEEE, 2003, pp. V–205.*
- [29] R. Schmidt, Multiple emitter location and signal parameter estimation, *IEEE transactions on antennas and propagation* 34 (3) (1986) 276–280.
- [30] M. Pesavento, A. B. Gershman, Z.-Q. Luo, Robust array interpolation using second-order cone programming, *IEEE Signal Processing Letters* 9 (1) (2002) 8–11.
- [31] B. K. Lau, G. J. Cook, Y. H. Leung, An improved array interpolation approach to doa estimation in correlated signal environments, in: *Acoustics, Speech, and Signal Processing, 2004. Proceedings.(ICASSP'04). IEEE International Conference on, Vol. 2, IEEE, 2004, pp. ii–237.*
- [32] B. K. Lau, M. Viberg, Y. H. Leung, Data-adaptive array interpolation for doa estimation in correlated signal environments, in: *Acoustics, Speech, and Signal Processing, 2005. Proceedings.(ICASSP'05). IEEE International Conference on, Vol. 4, IEEE, 2005, pp. iv–945.*
- [33] C.-L. Liu, P. Vaidyanathan, P. Pal, Coprime coarray interpolation for doa estimation via nuclear norm minimization, in: *Circuits and Systems (ISCAS), 2016 IEEE International Symposium on, IEEE, 2016, pp. 2639–2642.*
- [34] S. M. Hosseini, M. A. Sebt, Array interpolation using covariance matrix completion of minimum-size virtual array, *IEEE Signal Processing Letters* 24 (7) (2017) 1063.
- [35] M. A. Marinho, F. Antreich, J. P. C. da Costa, J. A. Nossek, A signal adaptive array interpolation approach with reduced transformation bias for doa estimation of highly correlated signals, in: *Acoustics, Speech and Signal Processing (ICASSP), 2014 IEEE International Conference on, IEEE, 2014, pp. 2272–2276.*
- [36] M. A. Marinho, J. P. C. da Costa, F. Antreich, A. L. de Almeida, Multidimensional array interpolation applied to direction of arrival estimation, in: *Smart Antennas (WSA 2015); Proceedings of the 19th International ITG Workshop on, VDE, 2015, pp. 1–6.*
- [37] M. A. Marinho, J. P. C. da Costa, F. Antreich, L. R. de Menezes, Unscented transformation based array interpolation, in: *Acoustics, Speech and Signal Processing (ICASSP), 2015 IEEE International Conference on, IEEE, 2015, pp. 2819–2823.*
- [38] M. A. Marinho, J. P. C. da Costa, F. Antreich, A. L. de Almeida, G. Del Galdo, E. P. de Freitas, A. Vinel, Array interpolation based on multivariate adaptive regression splines, in: *Sensor Array and Multichannel Signal Processing Workshop (SAM), 2016 IEEE, IEEE, 2016, pp. 1–5.*
- [39] M. S. Bartlett, Smoothing periodograms from time series with continuous spectra, *Nature* 161 (4096) (1948) 686–687.
- [40] S. Caizzone, A. Dreher, Miniaturized DRA array for GNSS applications, in: *Antennas and Propagation (EuCAP), 2015 9th European Conference on, IEEE, 2015, pp. 1–2.*

Appendix A. Proof of Theorem 1

Proof. Let a random variable \tilde{r} have a probability distribution function $p_{\tilde{r}}(r)$, $r \in \mathbb{R}$. Assuming that a moment generating function $M_{\tilde{r}}(k)$ exists, it is equivalent to the two-sided Laplace transform of \tilde{r} . Hence,

$$M_{\tilde{r}}(-k) = \mathcal{L}\{p_{\tilde{r}}(r)\}(k) + \mathcal{L}\{p_{\tilde{r}}(-r)\}(-k), \quad (\text{A.1})$$

where $\mathcal{L}\{p_{\tilde{r}}(r)\}(k)$ is the Laplace transform of $p_{\tilde{r}}(r)$. Thus, $M_{\tilde{r}}(-k)$ is unique iff both sides of the Laplace transform are unique. Therefore, since the Laplace transform of a function is unique, so is $M_{\tilde{r}}(-k)$. Thus, a PDF can be uniquely described by its moments provided that all moments exist and that $p_{\tilde{r}}(r)$ is integrable on any finite subset over its support. \square

Appendix B. Proof of Theorem 2

Proof. The log-likelihood can be given as

$$l(\mathbf{X}; \boldsymbol{\theta}, \phi) = -MN \log(\pi\sigma_n^2) - \frac{1}{\sigma_n^2} \text{tr} \{ (\mathbf{X} - \mathbf{A}\mathbf{S}) - (\mathbf{X} - \mathbf{A}\mathbf{S})^H \}, \quad (\text{B.1})$$

where $\text{tr}\{\cdot\}$ is the trace operator. Differentiating (B.1) with respect to σ_n^2 and equating to zero leads an estimate for the noise variance

$$\hat{\sigma}_n^2 = \frac{1}{MN} \text{tr} \{ (\mathbf{X} - \mathbf{A}\mathbf{S}) - (\mathbf{X} - \mathbf{A}\mathbf{S})^H \}. \quad (\text{B.2})$$

Substituting (B.2) into (B.1), differentiating with respect to \mathbf{S} , and equating to zero gives an estimate for \mathbf{S}

$$\hat{\mathbf{S}} = (\mathbf{A}^H \mathbf{A})^{-1} \mathbf{A}^H \mathbf{X}. \quad (\text{B.3})$$

Then, substituting (B.2) and (B.3) into (B.1) yields

$$\begin{aligned} (\hat{\boldsymbol{\theta}}, \hat{\phi}) &= \arg \max_{\boldsymbol{\theta}, \phi} \text{tr} \left\{ \mathbf{A}(\mathbf{A}^H \mathbf{A})^{-1} \mathbf{A}^H \hat{\mathbf{R}}_{\mathbf{X}\mathbf{X}} \right\} \\ &= \arg \max_{\boldsymbol{\theta}, \phi} l_c(\mathbf{X}; \boldsymbol{\theta}, \phi). \end{aligned} \quad (\text{B.4})$$

Assuming that the received signals have low spatial correlation with

$$\forall^d_{i, i' = 1} \mathbf{a}^H(\theta_i, \phi_i) \mathbf{a}(\theta_{i'}, \phi_{i'}) \rightarrow 0, \quad i \neq i' \quad (\text{B.5})$$

the concentrated loss function close to the global optimum can be approximated as

$$\begin{aligned} \arg \max_{\boldsymbol{\theta}, \phi} l_c(\mathbf{X}; \boldsymbol{\theta}, \phi) &\approx \arg \max_{\boldsymbol{\theta}, \phi} \sum_{i=1}^d \frac{\mathbf{a}^H(\theta_i, \phi_i) \hat{\mathbf{R}}_{\mathbf{X}\mathbf{X}} \mathbf{a}(\theta_i, \phi_i)}{\mathbf{a}^H(\theta_i, \phi_i) \mathbf{a}(\theta_i, \phi_i)} \\ &\approx \arg \max_{\boldsymbol{\theta}, \phi} \sum_{k=1}^K \frac{1}{\chi_k} P(\theta, \phi) |_{(\theta, \phi) \in \mathcal{S}_k}, \end{aligned} \quad (\text{B.6})$$

where with $\theta \in \mathcal{D}_{\Delta_\theta}$ and $\phi \in \mathcal{D}_{\Delta_\phi}$

$$\chi_k = \sum_{(\theta, \phi) \in \mathcal{S}_k} P(\theta, \phi) \Delta_\theta \Delta_\phi. \quad (\text{B.7})$$

\square

Remark 1. The assumption that signals have low spatial correlation can be found valid for many cases, especially, for arrays with $M \rightarrow \infty$. However, signals can still have high correlation in time with cross-correlation coefficient $\gamma_{i,i'} \rightarrow 1$.

Remark 2. The approximation introduced in (B.6) results to $\forall_{(\theta,\phi) \notin \mathcal{S}} l_c(\mathbf{X}; \boldsymbol{\theta}, \phi) \triangleq 0$. The normalization χ_k with respect to each sector \mathcal{S}_k makes it possible to consider the concentrated loss function for each sector \mathcal{S}_k as a separate PDF when applying the UT.